Defining and targeting tumor-associated macrophages in malignant mesothelioma

Wu, Licun ; Kohno, Mikihiro ; Murakami, Junichi ; Zia, Amin ; Allen, Jonathan ; Yun, Hana ; Chan, Meilin ; Baciu, Cristina ; Liu, Mingyao ; Serre-Beinier, Veronique ; De Palma, Michele ; Felley-Bosco, Emanuela ; Yeung, Jonathan ; Pugh, Trevor J ; de Perrot, Marc

DOI: https://doi.org/10.1073/pnas.2210836120

PNAS RESEARCH ARTICLE | IMMUNOLOGY AND INFLAMMATION OPEN ACCESS

Defining and targeting tumor-associated macrophages in malignant mesothelioma

Licun Wu[a,b], Mikihiro Kohno[a], Junichi Murakami[a], Amin Zia[a,c], Jonathan Allen[a], Hana Yun[a], Meilin Chan[a], Cristina Baciu[a], Mingyao Liu[a], Veronique Serre-Beinier[d], Michele De Palma[e,f], Emanuela Felley-Bosco[g], Jonathan Yeung[a], Trevor J. Pugh[b], and Marc de Perrot[a,b,h,1]

Edited by Harvey Cantor, Dana-Farber Cancer Institute, Boston, MA; received June 23, 2022; accepted November 7, 2022

Defining the ontogeny of tumor-associated macrophages (TAM) is important to develop therapeutic targets for mesothelioma. We identified two distinct macrophage populations in mouse peritoneal and pleural cavities, the monocyte-derived, small peritoneal/pleural macrophages (SPM), and the tissue-resident large peritoneal/pleural macrophages (LPM). SPM rapidly increased in tumor microenvironment after tumor challenge and contributed to the vast majority of M2-like TAM. The selective depletion of M2-like TAM by conditional deletion of the Dicer1 gene in myeloid cells ($D^{-/-}$) promoted tumor rejection. Sorted SPM M2-like TAM initiated tumorigenesis in vivo and in vitro, confirming their capacity to support tumor development. The transcriptomic and single-cell RNA sequencing analysis demonstrated that both SPM and LPM contributed to the tumor microenvironment by promoting the IL-2-STAT5 signaling pathway, inflammation, and epithelial–mesenchymal transition. However, while SPM preferentially activated the KRAS and TNF-α/NFkB signaling pathways, LPM activated the IFN-γ response. The importance of LPM in the immune response was confirmed by depleting LPM with intrapleural clodronate liposomes, which abrogated the antitumoral memory immunity. SPM gene signature could be identified in pleural effusion and tumor from patients with untreated mesothelioma. Five genes, *TREM2, STAB1, LAIR1, GPNMB*, and *MARCO*, could potentially be specific therapeutic targets. Accordingly, Trem2 gene deletion led to reduced SPM M2-like TAM with compensatory increase in LPM and slower tumor growth. Overall, these experiments demonstrate that SPM M2-like TAM play a key role in mesothelioma development, while LPM more specifically contribute to the immune response. Therefore, selective targeting of monocyte-derived TAM may enhance antitumor immunity through compensatory expansion of tissue-resident TAM.

tumor-associated macrophages | tumor microenvironment | mesothelioma | gene signature | cancer

Significance

Tumor-associated macrophages (TAM) contribute to the immunosuppressive microenvironment of mesothelioma. We focused on the distinct subsets of small and large peritoneal/pleural macrophages (SPM and LPM) to identify their gene signatures. SPM preferentially contribute to M2-like phenotype, while LPM more specifically contributed to the immune response. *TREM2, STAB1, LAIR1, GPNMB,* and *MARCO* could potentially provide specific therapeutic targets.

Although mesothelioma carries poor prognosis, genomic alterations have helped to identify new therapeutic targets and isolate markers associated with better prognosis (1). Mesothelioma occurring in the context of germline mutations can also have better survival, of up to 20 y on rare occasions (2). Mesothelioma is composed of a variety of tumor-infiltrating cells (3–6). Tumor-associated macrophages (TAM) in particular can generate an immunosuppressive tumor microenvironment, initiate angiogenesis, and facilitate cancer cell motility (7). Different subpopulations of TAM can be detected in the tumor microenvironment, some deriving from circulating monocytes, while others deriving from local tissue microenvironment. Monocyte-derived TAM are immunosuppressive and, therefore, erect barriers to effective immunotherapy (8). Resident or tissue macrophages play various roles in maintaining tissue homeostasis and immune surveillance. However, their specific role in tumor development is not well characterized.

Peritoneal macrophages encompass two distinct populations based on their size, small peritoneal macrophages (SPM) and large peritoneal macrophages (LPM) (9, 10). SPM originate from monocytes, while LPM are predominantly resident macrophages of embryonic origin (11, 12). Monocyte-derived macrophages and tissue-resident macrophages are also generally characterized by distinct cluster of differentiation 11b (CD11b) and F4/80 expression patterns (13–16). The distinction between SPM and LPM provides the unique opportunity to determine their specific contribution to the development of mesothelioma and to identify specific therapeutic targets (17–19). In this study, we investigated the dynamics, role, and gene expression profiles of SPM and LPM during mesothelioma development.

Results

Dynamics of TAM Subpopulations during Mesothelioma Development. In order to determine the importance of each macrophage subpopulation, we performed a time course to characterize the infiltration of SPM and LPM in peritoneal lavage during

Author contributions: L.W., E.F.-B., J.Y., and M. de Perrot designed research; L.W., M.K., J.M., H.Y., M.C., V.S.-B., and E.F.-B. performed research; M.L., M. De Palma, and T.J.P. contributed new reagents/analytic tools; L.W., M.K., J.M., A.Z., J.A., H.Y., M.C., C.B., V.S.-B., E.F.-B., and J.Y. analyzed data; J.A. and C.B. discussion about the data presentation; M.L. and T.J.P. participated in study discussion; M.D. participated in study discussion and manuscript editing; J.Y. participation in manuscript discussion; M. de Perrot interpretation of the results; L.W. and M. de Perrot wrote the paper.

Competing interest statement: The authors have organizational affiliations to disclose. M. De Perrot received personal fees outside of this work from Bayer (speaking fees for work related to pulmonary hypertension), Merck (speaking fees for work related to lung cancer), Janssen (consulting fees for work related to pulmonary hypertension), Roche (consulting fees for work related to lung cancer), BMS (consulting fees for work related to lung cancer), and Astra-Zeneca (Ad board for work related to lung cancer).

This article is a PNAS Direct Submission.

[1]To whom correspondence may be addressed. Email: marc.deperrot@uhn.ca.

This article contains supporting information online at https://www.pnas.org/lookup/suppl/doi:10.1073/pnas.2210836120/-/DCSupplemental.

Published February 23, 2023.

development and progression of mesothelioma using an established mouse model (20) (Fig. 1*A*). Single cells from peritoneal lavage contained immune infiltrates including monocytes, TAM, T, and B lymphocytes. The proportions of T and B cells were found to increase in peritoneal lavage at the end of the first week after tumor cell injection and decreased afterward (*SI Appendix*, Fig. S1). Two TAM populations were observed from day 7 up to the end of observation on day 28 (Fig. 1*B*). The SPM population (characterized by $CD11b^{lo}F4/80^{lo}$) rapidly increased within the first week after tumor challenge and remained stable afterward. Conversely, the LPM population (characterized by $CD11b^{hi}F4/80^{hi}$) slowly increased over the 4-wk period (Fig. 1*C*). Fluorescent immunostaining with CD11b and F4/80 confirmed the presence of SPM and LPM in peritoneal lavage (Fig. 1*D*).

Monocyte-Derived SPM Are Predominantly M2-Like Macrophages. We then used an intrapleural mesothelioma model to confirm that a similar time course occurred in the pleural cavity after mesothelioma cell challenge (21). Since tumor progression is faster in the pleural cavity than the peritoneal cavity, the time course was over 14 d. We observed a rapid accumulation of SPM on day 3 after tumor challenge. This population remained stable over time, while the LPM subpopulation rapidly dropped after day 10 (Fig. 1*E*). SPM expressed $CD206^+$ on day 10 and represented about 80% of the $CD206^+$ TAM population. By day 14, the LPM population had almost disappeared, and therefore, SPM were nearly the only population of $CD206^+$ TAM in the pleural lavage (Fig. 1*F*). Looking at myeloid-derived suppressor cells (MDSC), we observed a rapid accumulation of inflammatory monocytes (MMDSC) characterized by $CD11b^+Ly6C^+Ly6G^-$ on day 7 after tumor cell injection, while granulocytic-MDSC characterized by $CD11b^+Ly6C^-Ly6G^+$ (PMN-MDSC) increased in large proportion on days 10 and 14 (*SI Appendix*, Fig. S2). This time course supports the possibility that M-MDSC transformed into polymorphonuclear (PMN)-MDSC (22, 23).

Overall, the time course demonstrated that the SPM population rapidly increased after tumor challenge and that the vast majority of M2-like TAM were SPM. All mice died within 3 wk in the intrapleural model correlating with a rapid drop in LPM at 2 wk. In contrast, survival lasted 5 to 6 wk in the intraperitoneal model and corresponded with rise in the LPM population after 2 wk. Considering the longer survival and the persistence of both SPM and LPM subpopulations, the peritoneal model was used in most of the following experiments.

Systemic Depletion of Macrophages by Clodronate Liposomes (CL) Decreased Tumorigenicity, Mesothelial Progenitor Cells, and Cytokine Release. To determine the importance of TAM in tumor development, macrophages were depleted by CL on the same day as the tumor challenge. Both M1-like inducible Nitric oxide synthase ($iNOS^+$) and M2-like ($Arg1^+$/$CD206^+$) phenotypes were depleted by CL (*SI Appendix*, Fig. S3). Macrophage depletion was associated with a significant drop in total macrophages (major histocompatibility complex class II $(MHCII)^+CD68^+F4/80^+$) and mesothelial precursor cells ($Msln^+CD34^+CD90^+$) in the peritoneal lavage (Fig. 2 *A* and *B*). Previous work had shown that mesothelial precursor cells were detectable in the circulation during the development of mesothelioma and increased in parallel to macrophages in the peritoneal cavity, suggesting an interconnectivity between these two populations (20, 24–26). The number of spheroids in the peritoneal lavage at 4 wk and 6 wk after macrophage depletion also dropped but were still detectable (Fig. 2*C*). Tumor invasion into the diaphragm was absent in CL-treated group, while it was evident in control mice at 4 wk after tumor challenge (Fig. 2 *D* and *E*). Inflammatory and immune cytokines in the peritoneal lavage at 4 wk after *ip* injection of tumor cells were significantly lower after macrophage depletion compared to control (*SI Appendix*, Fig. S4). Chemokine (C-C motif) ligand 2 (CCL2) remained high compared to tumor-naïve mice demonstrating that CCL2 production was independent of macrophage upregulation.

Loss of Antitumoral Memory T Cell Protection after Systemic Depletion of Macrophages by CL. CL depleted both SPM and LPM, and we therefore questioned whether the systemic depletion of macrophages could attenuate the memory antitumoral immune response. We had demonstrated in a *sc* mouse mesothelioma model that a short course of radiation followed by surgical resection of the tumor 7 d later led to an in situ vaccination with long-term immune memory protection mediated by $CD4^+$ T cells (27). This memory model provided intrapleural protection with rapid rise of antitumoral memory T cells after tumor challenge in the pleural cavity leading to tumor rejection (28). We therefore tested the impact of macrophage depletion with CL injection in the pleural cavity using this model. CL led to rapid depletion of SPM and LPM in the pleural cavity by day 3 after injection. By day 10, however, LPM remained absent in the pleural cavity, but MMDSC and SPM were present (Fig. 2*F*). The T cell population was maintained in the spleen after CL injection (*SI Appendix*, Fig. S5). Using the memory model, mice were challenged by intrapleural injection of mesothelioma cancer cells. Memory mice rejected the tumor and survived for at least 60 d after tumor rechallenge. In contrast, memory mice that were injected with CL developed intrathoracic mesothelioma and died after 30 d from tumor progression (Fig. 2*G*). Despite tumor progression in the pleural cavity, memory mice treated with CL survived longer than naïve mice supporting a persistent protection from memory T cells. Naïve mice treated with CL tended to die faster than untreated mice after tumor challenge.

Taken together, these results demonstrate that macrophages contribute to the immune memory protection, and therefore, nonspecific depletion of macrophages may be detrimental and limit the immune response against the tumor. Recent evidence supports this observation by demonstrating that resident macrophages colocalize with memory CD4 T cells to generate an adequate memory response (29).

Selective Depletion of M2-Like Macrophages Results in Tumor Rejection in *Dicer1*-Deficient Macrophages with Near Normalization of the Gene Expression Profile in the Tumor Microenvironment. Considering the importance of selective macrophage depletion to mediate the most benefit in cancer therapy, we next specifically focused on depleting M2-like macrophages by using mice with myeloid-specific inactivation of the *Dicer1* gene ($D^{-/-}$) (30). After tumor challenge in the *ip* model, intraperitoneal mesospheres in $D^{-/-}$ mice were absent in the majority of the mice at 4 wk and 6 wk after RN5 cells *ip* injection (Fig. 3*A*). M2-polarized macrophages were depleted in the peritoneal lavage of $D^{-/-}$ mice compared with $D^{+/+}$ mice (Fig. 3*B*), while in the *sc* model, tumor growth was palpable 1 wk after tumor cell injection, but then the tumor was completely rejected in $D^{-/-}$ mice, while it continued to grow in $D^{+/+}$ mice (Fig. 3*C*). Using *ip* model, we observed that both SPM and LPM populations significantly dropped in tumor-bearing $D^{-/-}$ mice (Fig. 3*D*). The drop was more pronounced in SPM compared to LPM and the $CD206^+$.

SPM were nearly completely absent (Fig. 3*E*). The immune checkpoint programmed death ligand 1 (PD-L1) was also nearly absent on TAM in $D^{-/-}$ mice at 4 wk after tumor cell injection (Fig. 3*E* and *SI Appendix*, Fig. S6). Most importantly, the peritoneal lavage from $D^{-/-}$ tumor-bearing mice demonstrated that the gene expression profile had almost normalized in $D^{-/-}$ mice compared to naïve mice with only 158 genes that were up or downregulated, while

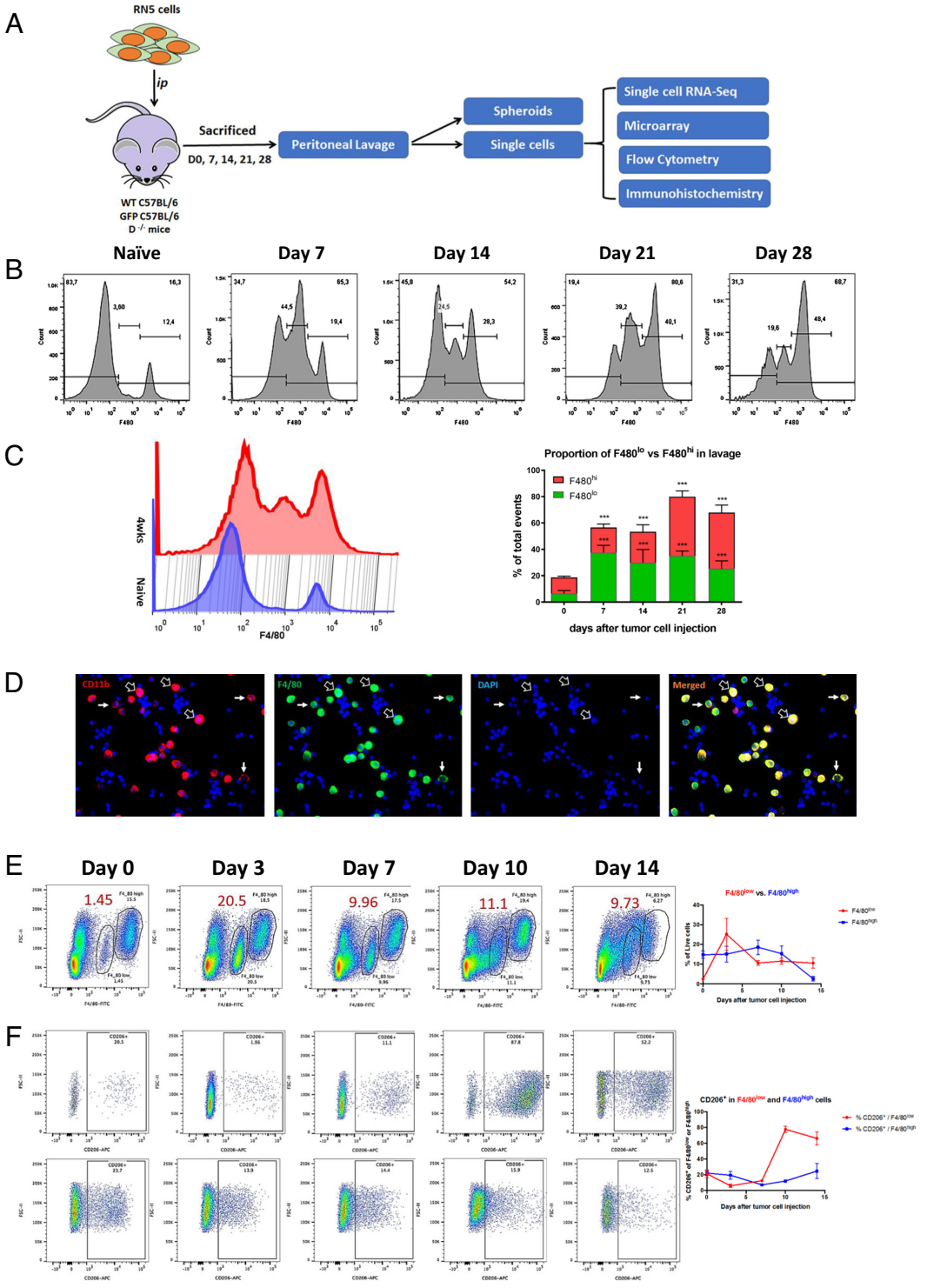

Fig. 1. Experimental design of intraperitoneal and intrapleural mesothelioma models in mice. (*A*) Schema of the experimental design in intraperitoneal mouse model: RN5 cells (2×10^6) were injected intraperitoneally (*ip*) into C57BL/6 mice, lavage rinsed with phosphate buffered saline (PBS) was collected at different time points, single cells were used for further analysis. (*B*) Two distinct subpopulations of TAM were identified by F4/80^{hi}CD11b^{hi} (LPM) and F4/80^{lo}CD11b^{lo} (SPM). (*C*) Total macrophages, including SPM and LPM populations, accumulated in the peritoneal cavity after tumor challenge and were quantitatively analyzed up to day 28. (*D*) Fluorescent immunostaining of SPM (CD11b^{lo}F4/80^{lo}) and LPM (CD11b^{hi}F4/80^{hi}) from tumor-bearing mice at 4 wk after tumor cell injection. (*E*) Intrapleural mouse model: AB12 cells (5×10^5) were injected intrapleurally into Balb/c mice. Representative dot plots of flow cytometry in the intrapleural model. (*F*) The proportions of CD206 in SPM and LPM were presented during observation after tumor challenge. **P* < 0.05, ***P* < 0.01, ****P* < 0.001, *****P* < 0.0001.

tumor-bearing wild-type (WT) mice had 3,314 genes that were dysregulated compared to naïve mice (Fig. 3*F*). The top 10 pathways that were dysregulated in WT tumor-bearing mice were the T cell receptor (TCR) and B cell receptor (BCR) signaling pathways, tumor growth factor β (TGF-β) receptor signaling pathway, Wnt signaling pathway, and p53 signaling pathway (Fig. 3*G*). These pathways were reversed to normalization in D$^{-/-}$ mice (*SI Appendix*, Fig. S7). One of the pathways that remained dysregulated in D$^{-/-}$ mice was the phosphoinositide-3-kinase-protein kinase B (also known as Akt)-mammalian target of rapamycin (PI3k-Akt-mTOR) signaling pathway.

Taken together, these results demonstrate that the polarization of SPM into M2-like TAM is a critical step in the development

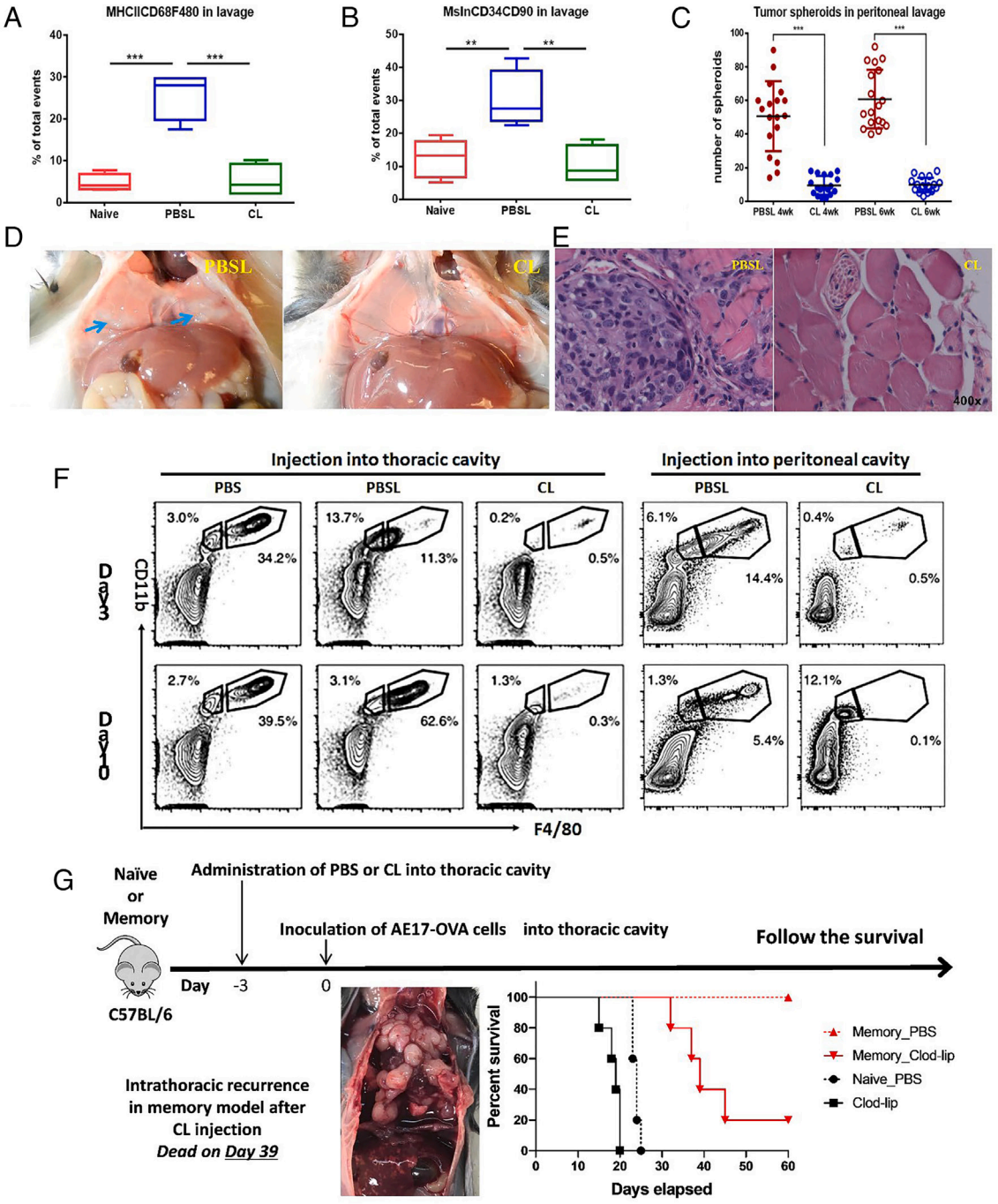

Fig. 2. Systemic depletion of TAM resulted in a significant decrease in mesothelial precursor cells in peritoneal lavage, mesospheres, and tumorigenicity. (*A* and *B*) Macrophages were depleted by CL on the same day as tumor challenge. Macrophage depletion was associated with a significant reduction in total macrophages ($MHCII^+CD68^+F4/80^+$) and mesothelial precursor cells characterized by $Msln^+CD34^+CD90^+$ in the peritoneal lavage. (*C*) The number of spheroids in the peritoneal lavage at 4 wk and 6 wk after treatment with CL compared with PBS liposome (PBSL) was counted based on the diameter greater than 100 μm. (*D* and *E*) Tumor invasion into the diaphragm was evident at 4 wk after *ip* injection of RN5 cells in control mice, while it was absent in CL-treated group. (*F*) The impact of macrophage depletion with CL injection in the pleural cavity was tested in the intrapleural model. PBS, PBSL, or CL was injected into the thoracic cavity and peritoneal cavity of naïve mice, respectively, and mice were killed on day 3 and day 10. The depletion of SPM and LPM was quantified in both models. (*G*) Using the memory model, mice were then challenged by intrapleural injection of mesothelioma cells. Survival time and tumor progression were recorded in memory mice with or without CL treatment in response to the tumor rechallenge. *$P < 0.05$, **$P < 0.01$, ***$P < 0.001$, ****$P < 0.0001$.

of mesothelioma. The depletion of M2-like TAM remains associated with a dysregulated PI3k-Akt-mTOR signaling pathway, suggesting that targeting this pathway in combination with M2-like TAM depletion could be beneficial.

In the next series of experiments, we isolated SPM M2-like TAM to confirm their critical role in mesothelioma development and identified a specific gene signature profile to characterize SPM.

Sorted SPM M2-Like Macrophages from Peritoneal Lavage of WT and GFP Tumor-Bearing Mice Initiate Tumorigenesis. Peritoneal lavage cells were collected from the RN5-bearing WT mice at 4 wk after ip injection. Sorted M2-like SPM cells ($CD11b^{lo}F4/80^{lo}CD206^+$) were then injected *sc* and *ip* into WT mice, where tumors and mesospheres were formed respectively (Fig. 4*A*). Tumors and mesospheres were confirmed by immunostaining with WT1 and Ki67 (Fig. 4*B*). A similar

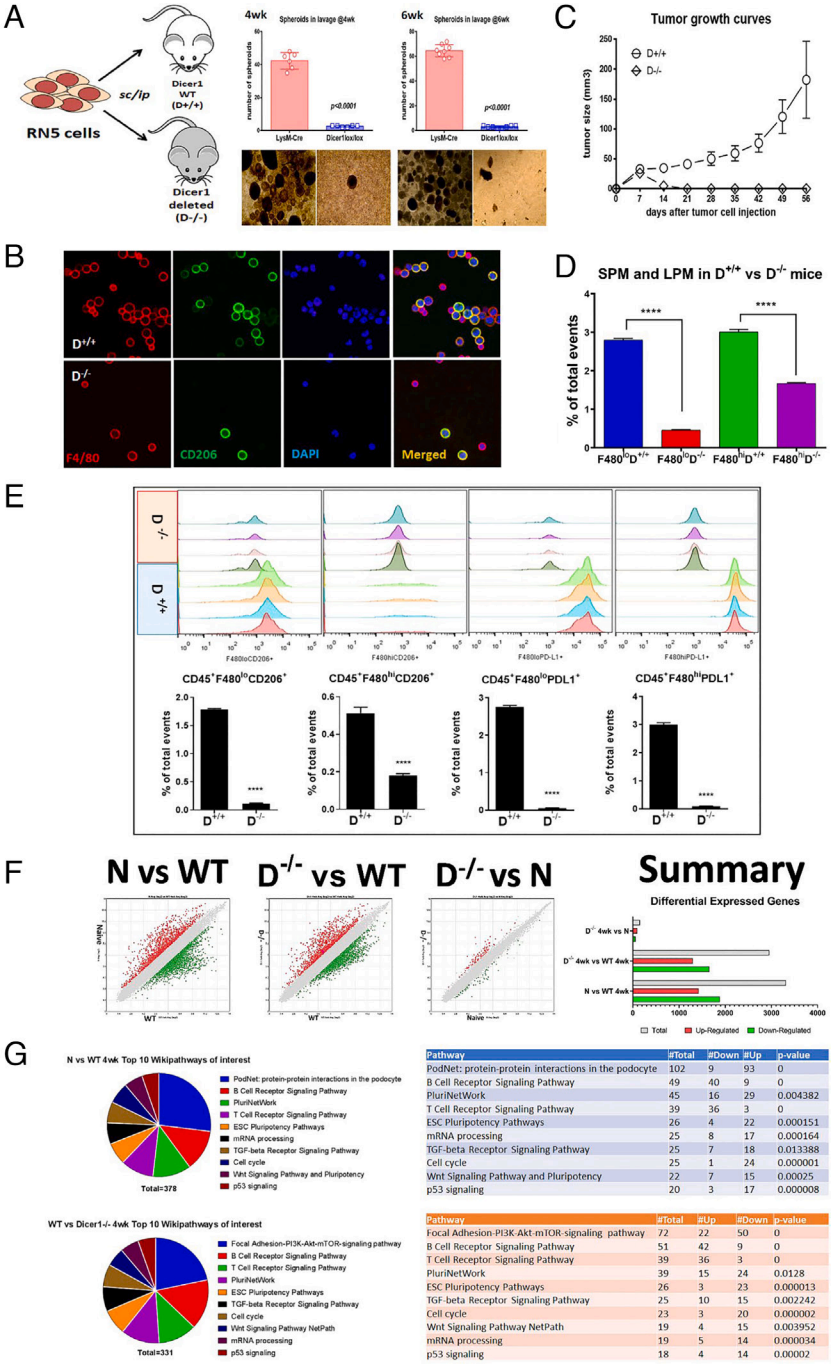

Pathway	#Total	#Down	#Up	p-value
PodNet: protein-protein interactions in the podocyte	102	9	93	0
B Cell Receptor Signaling Pathway	49	40	9	0
PluriNetWork	45	16	29	0.004382
T Cell Receptor Signaling Pathway	39	36	3	0
ESC Pluripotency Pathways	26	4	22	0.000151
mRNA processing	25	8	17	0.000164
TGF-beta Receptor Signaling Pathway	25	7	18	0.013388
Cell cycle	25	1	24	0.000001
Wnt Signaling Pathway and Pluripotency	22	7	15	0.00025
p53 signaling	20	3	17	0.000008

Pathway	#Total	#Up	#Down	p-value
Focal Adhesion-PI3K-Akt-mTOR-signaling pathway	72	22	50	0
B Cell Receptor Signaling Pathway	51	42	9	0
T Cell Receptor Signaling Pathway	39	36	3	0
PluriNetWork	39	15	24	0.0128
ESC Pluripotency Pathways	26	3	23	0.000013
TGF-beta Receptor Signaling Pathway	25	10	15	0.002242
Cell cycle	23	3	20	0.000002
Wnt Signaling Pathway NetPath	19	4	15	0.003952
mRNA processing	19	5	14	0.000034
p53 signaling	18	4	14	0.00002

Fig. 3. Selective depletion of TAM resulted in a significant decrease in mesospheres in peritoneal lavage and unfavorable tumorigenicity. (*A*) Selective depletion of M2-like SPM macrophages was achieved in $D^{-/-}$ mice. Macrophage M2-like depletion by using Dicer1-deficient ($D^{-/-}$) mice to inject tumor cells in the *ip* model, the number of intraperitoneal mesospheres in the $D^{+/+}$ and $D^{-/-}$ mice was counted at 4 wk and 6 wk after RN5 cells *ip* injection. (*C*) In the *sc* model, tumor growth was initiated and palpable for the first few days after tumor challenge in both groups, but then the tumor was completely rejected in $D^{-/-}$ mice, while it continued to grow in $D^{+/+}$ mice. (*B*) The M2-polarized macrophages in the peritoneal lavage of $D^{-/-}$ mice compared with $D^{+/+}$ mice were identified with $F4/80^{lo}CD206^{+}$ fluorescent immunostaining. (*D*) Using *ip* model, both SPM and LPM populations significantly dropped in tumor-bearing $D^{-/-}$ mice. (*E*) The immune checkpoint PD-L1 was remarkably reduced in TAM of tumor-bearing $D^{-/-}$ mice compared with $D^{+/+}$ mice. The majority $CD206^{+}$ M2-like macrophages were SPM in $D^{+/+}$ mice. $CD206^{+}$ SPM were nearly absent in $D^{-/-}$ mice. PD-L1 was downregulated in all TAM in $D^{-/-}$ mice at 4 wk after tumor cell injection. (*D*) $D^{-/-}$ resulted in drop of SPM and LPM, but to a much larger extent in SPM (*E*). (*F*) Total number of genes with significant differential expression. Nearly all differentially expressed genes were converted to normal in $D^{-/-}$ mice compared with tumor-naïve mice. (*G*) Top 10 WikiPathways of interest in comparing: Naïve vs. WT (*Top*), WT $D^{+/+}$ vs. $D^{-/-}$ (*Bottom*). $^{*}P < 0.05$, $^{**}P < 0.01$, $^{***}P < 0.001$, $^{****}P < 0.0001$.

experiment was then performed in green fluorescent protein (GFP) mice to confirm the purity of $GFP^{+}F4/80^{lo}CD206^{+}$ after cell sorting and track the GFP expression. M2-like SPM macrophages were able to form spheroids at day 14 (Fig. 4 *C* and *D*). Sorted cells were GFP^{+} at the beginning of the culture and disappeared after the first passage. When the isolated $GFP^{+}F4/80^{lo}CD206^{+}$ M2-like SPM were injected *sc* into mice, solid tumors developed with similar properties as parental RN5 cells. Whole-genome sequencing data showed that the genetic profile was nearly identical between the new cell lines and the original RN5 cell population (*SI Appendix*, Fig. S8). The same number of $F4/80^{hi}CD206^{-}$ sorted cells were injected *sc* but did not induce tumors after 3 mo of observation. These results demonstrate that M2-like SPM TAM facilitate tumor development, supporting an autoregulatory loop between TAM and cancer cells in protumorigenic niche leading cancer cells to acquire stem cell characteristics (8, 31).

Transcriptomic Analysis of TAM Subpopulations by Microarray. Considering that SPM and LPM had different ability to become M2-like TAM and had a different impact on tumor growth and tumor immune response, we analyzed the gene expression profile of SPM and LPM using transcriptomic analysis. We selected the 4-wk time point to perform the microarray analysis.

Total RNAs extracted from $CD11b^{lo}F4/80^{lo}$ (SPM) and $CD11b^{hi}F4/80^{hi}$ (LPM) subpopulations of sorted cells were used to perform Affymetrix microarray. SPM were compared to LPM in tumor-bearing mice and in tumor-naive mice. Up- or down-regulated genes were shown in scatter plots (Fig. 5*A*). The differentially expressed genes were then summarized (Fig. 5*B*). Comparison between SPM and LPM from tumor-bearing mice included 421 (1.22%) genes that passed filter criteria among which 200 (47.51%) were upregulated and 221 (52.49%) genes were downregulated (*SI Appendix*, Fig. S9).

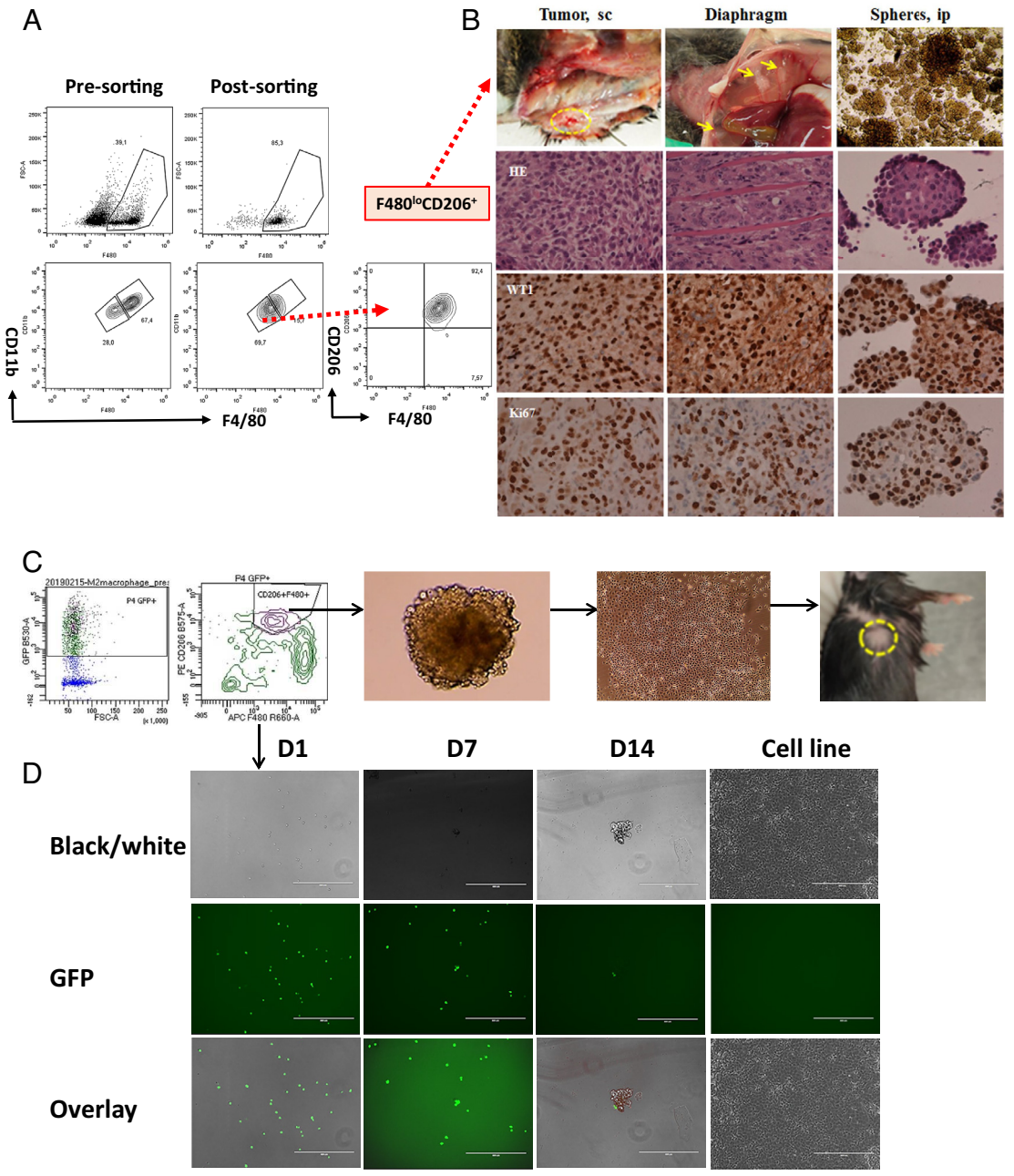

Fig. 4. Sorted M2-like SPM macrophages from peritoneal lavage of RN5-bearing WT or GFP mice initiate tumorigenesis. (*A*) Peritoneal lavage cells were collected from the RN5-bearing WT mice at 4 wk after *ip* injection. F4/80^{lo}CD11b^{lo}CD206^{+} cells were sorted using a cell sorter. (*B*) Sorted SPM M2-like cells were injected subcutaneously and intraperitoneally into WT mice. Tumors and mesospheres were stained for H&E, WT1, and Ki67. (*C*) Similar experiment was then performed in GFP mice to confirm the purity of GFP^{+}F4/80^{lo}CD206^{+} after cell sorting by tracking GFP expression. Cell sorting strategy to acquire GFP^{+}F4/80^{lo}CD206^{+} M2-like SPM macrophages. M2-like SPM macrophages were able to form spheroids at day 14 and cell lines were derived from the spheroids. (*D*) Sorted cells were cultured in an ultra-low adherent plate. Spheroids were formed at day 14. Cell line was then established from the spheroids. Sorted cells were GFP^{+} at the beginning of culture and disappeared afterward.

Venn diagram indicated that SPM and LPM shared 855 genes (48.7%), while 557 genes were SPM-specific genes (32.9%) and 323 genes were LPM-specific genes (18.4%) (*SI Appendix*, Fig. S10). Gene set enrichment analysis (GSEA) was used to identify the top 10 hallmark gene sets that were specific for SPM (Fig. 5*C*), specific for LPM (Fig. 5*D*), and common to both SPM and LPM (Fig. 5*E*). Transcriptomic analysis showed that SPM-specific genes were involved in 155 WikiPathways, LPM-specific genes in 140 WikiPathways, and that common genes were involved in 95 WikiPathways (Dataset S1).

Single-Cell RNA Sequencing (scRNA-Seq) Identifies Specific Gene Signatures for SPM and LPM. Further characterization of SPM and LPM was performed by scRNA-Seq to identify specific markers for both TAM subpopulations. Specified clusters were highlighted with low or high expression of the gene *Adgre1* (Adgre1^{lo}, SPM or Adgre1^{hi}, LPM) encoding F4/80 in the peritoneal lavage from tumor-bearing mice and tumor-naive mice (Fig. 6*A*). *Adgre1* (F4/80) and *Itgam* (CD11b) had similar expression profiles, and we therefore used *Adgre1* to separate the subpopulations of TAM (*SI Appendix*, Fig. S11). As expected, the total number of macrophages (*Adgre1*$^{+}$) and both subpopulations of SPM and LPM were much higher in tumor-bearing mice than in tumor-naive mice (Fig. 6*B*). All subpopulations of macrophages were included in both groups to generate a heatmap of the top 50 up- or downregulated gene expression (Fig. 6*C*).

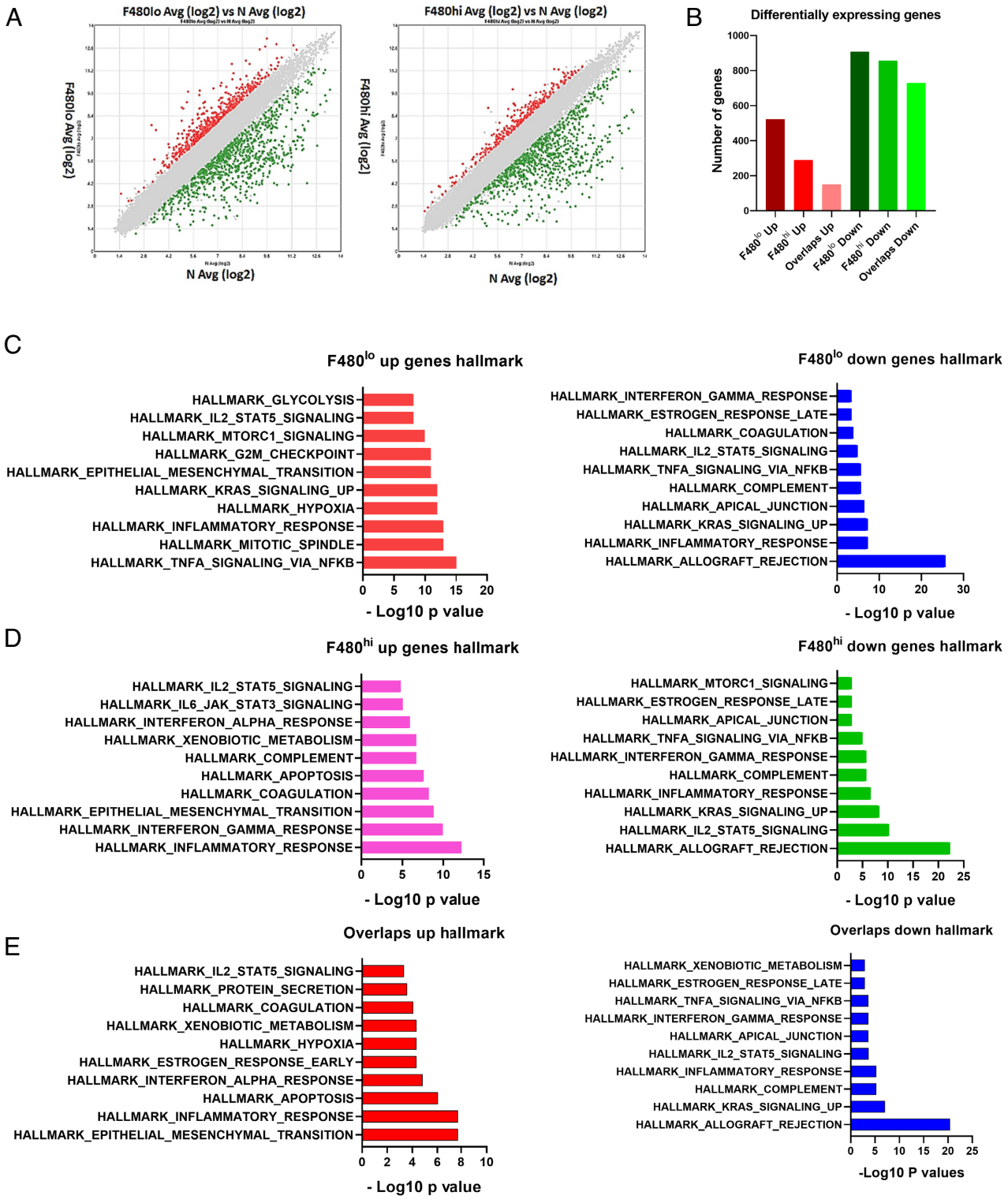

Fig. 5. Transcriptomic analysis of gene expression profiles of SPM and LPM by microarray. (*A*) Total RNAs extracted from CD11b^{lo}F4/80^{lo} (SPM) and CD11b^{hi}F4/80^{hi} (LPM) subpopulations of sorted cells were used to perform Affymetrix microarray. Naïve group was included for controls. SPM were compared to LPM in tumor-bearing mice and tumor-naive mice, and up- or downregulated genes were shown in scatter plots as average values (log2). (*B*) Summary of differentially expressed genes, red color represents upregulated genes and green color downregulated genes. (*C*) GSEA was performed to show the SPM-specific genes involved in top 10 hallmark gene sets of up- or downregulated genes (>twofold change; $P < 0.05$). (*D*) LPM-specific genes involved in top 10 hallmark gene sets, and (*E*) common genes shared by both subpopulations involved in top 10 hallmark gene sets.

Overlapping genes between SPM and LPM in RN5-bearing mice or tumor-naïve mice were excluded using the Gene List Venn Diagram (www.bioinformatics.org/gvenn/) by importing all genes with significant change (>twofold change and $P < 0.05$) (Fig. 6*D*). A specific gene signature of SPM and LPM in naive and RN5 mice was then selected from the gene lists (Fig. 6*E*).

Common genes in SPM and LPM from both naïve and RN5 mice were also identified (*SI Appendix*, Fig. S12).

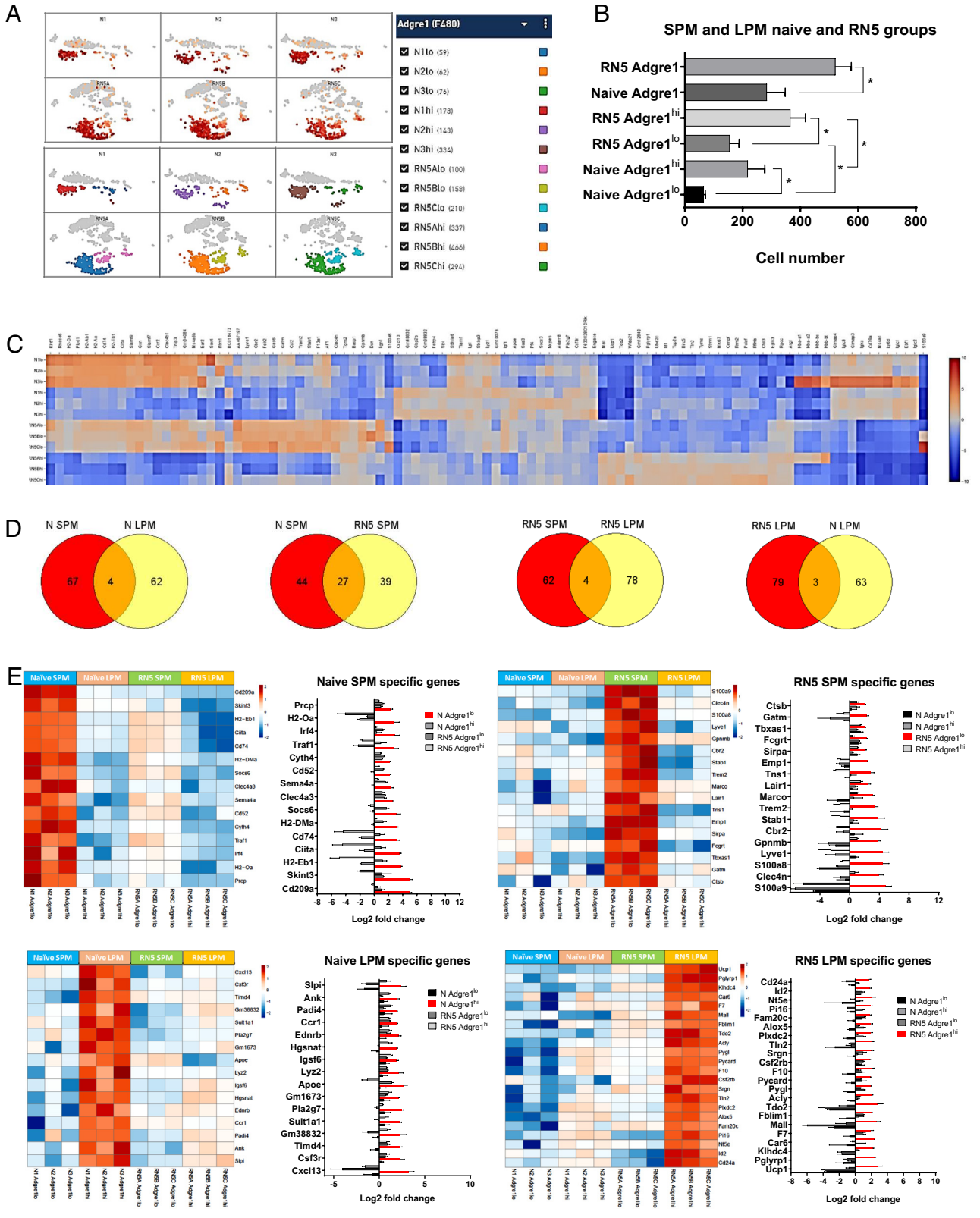

Fig. 6. Gene signatures of SPM and LPM identified by scRNA-Seq. (*A*) The gene *Adgre1* (encoded protein F4/80) expression in single cells from treatment-naïve and RN5-bearing mice. Adgre1lo and Adgre1hi cells in all clusters were highlighted with different colors. (*B*) SPM and LPM populations increased significantly in RN5 compared with treatment-naïve mice. (*C*) Heatmap of differentially expressed genes in SPM, LPM of treatment-naïve and RN5 groups plotted by Loupe Cell Browser. (*D*) Venn diagrams show the number of genes specific for each population or shared between the two subpopulations. (*E*) Lists of specific genes for each population. Naïve SPM-specific genes, RN5 SPM-specific genes, Naïve LPM-specific genes, and RN5 LPM-specific genes were presented in both heatmaps and bar graphs (genes of interest shown in red). **P* < 0.05, ***P* < 0.01, ****P* < 0.001, *****P* < 0.0001.

Hallmark Gene Set Analysis Identifies Common and Different Pathways for SPM and LPM TAM Subpopulations. Hallmark gene sets were determined by GSEA/MSigB software. The list of differentially upregulated genes generated from microarray and scRNA-Seq data was imported to the pathway analysis of GSEA and Gene Ontology database. The top 10 hallmark gene sets from the microarray data

were compared to the top 10 hallmark gene sets from scRNA-Seq data for both SPM and LPM (*SI Appendix*, Fig. S13 and Tables S1–S4).

SPM-specific hallmark gene sets common to both microarray data and scRNA-seq data demonstrated activation of the Kirsten rat sarcoma virus (KRAS) and tumor necrosis factor α (TNF-α) via nuclear factor kB (NFkB) signaling pathway, while LPMspecific hallmark gene sets demonstrated activation of the coagulation cascade, complement factors and interferon γ (IFN-γ) response. Three common hallmark gene sets were identified for both SPM and LPM and included Interleukin 2-Signal transducer and activator of transcription 5 (IL-2-STAT5) signaling, inflammatory response, and epithelial–mesenchymal transition (EMT) (*SI Appendix*, Figs. S13 and S14).

SPM Gene Signature Is Present in Pleural Effusion and Tumor from Patients with Pleural Mesothelioma. scRNA-Seq of pleural effusion and tumor biopsy from five patients with pleural mesothelioma

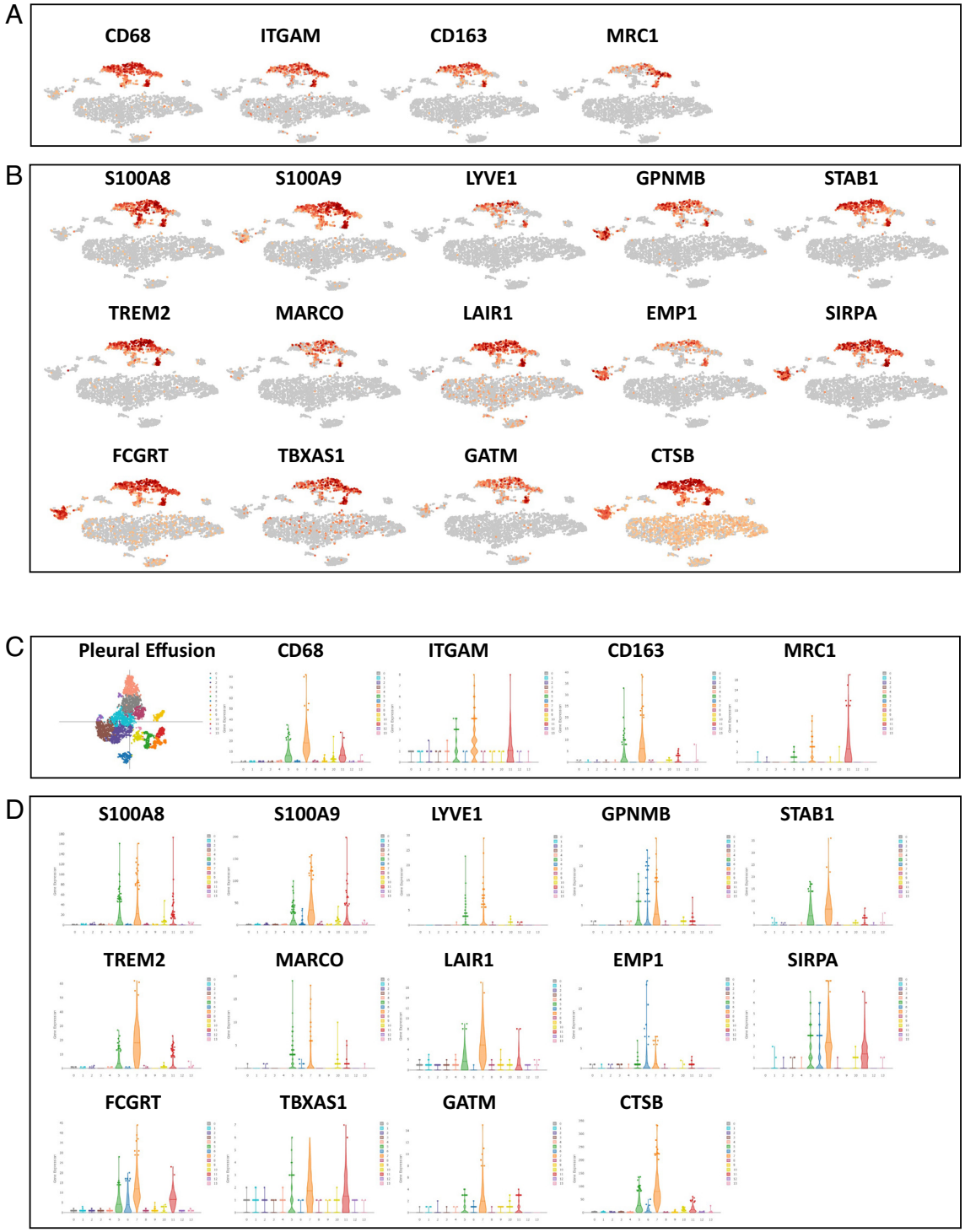

Fig. 7a. SPM gene signature is consistently identified in patients with mesothelioma, while LPM gene signature displays high variability. (*A*) Pleural effusion from a patient with malignant pleural mesothelioma. The t-SNE plots of macrophage cluster distribution (clusters 5, 7, and 11) identified by genes *CD68 ITGAM CD163* and *MRC1* showed dramatic overexpression of 14 SPM genes in both pleural effusion and tumor tissue of patients with pleural mesothelioma (*A* and *B* and *SI Appendix*, Fig. S15). Gene expression violin plots of SPM genes were consistently higher in macrophages than in other clusters in both pleural effusion and tumors (*C* and *D* and *SI Appendix*, Fig. S15).

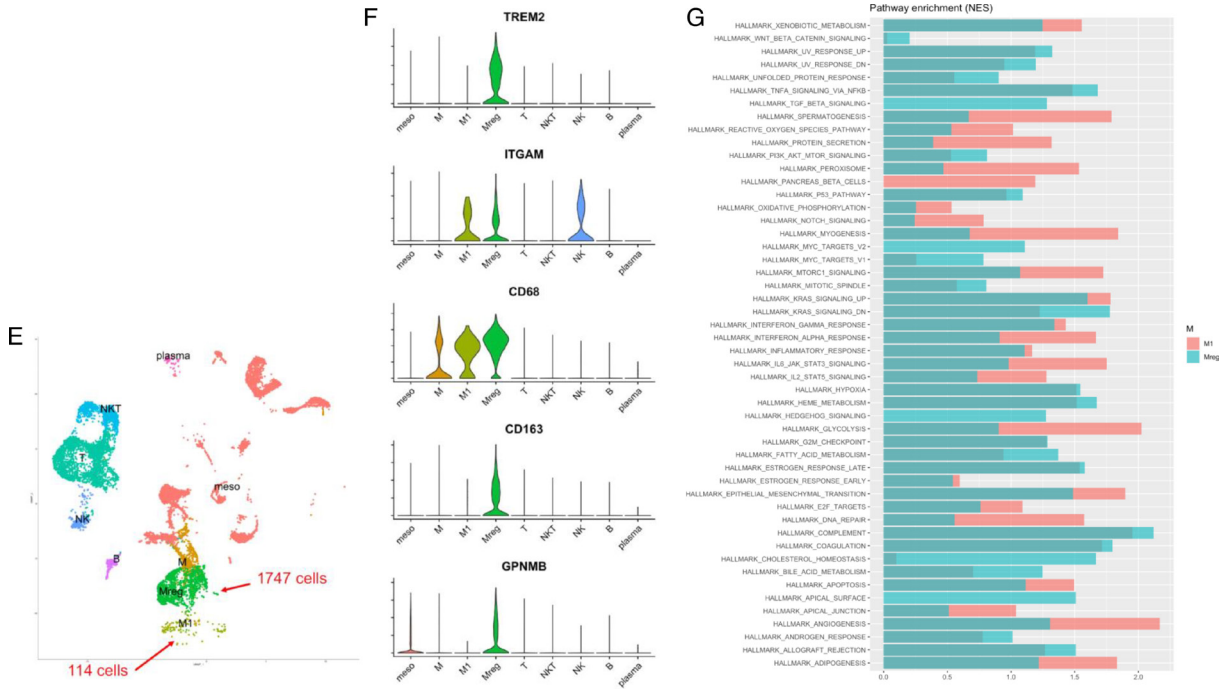

Fig. 7b. SPM gene signature is consistently identified in patients with mesothelioma, while LPM gene signature displays high variability. (*E*) Uniform manifold approximation and projection (UMAP) of single cells derived from tumor biopsy of untreated mesothelioma. Regulatory macrophages (Mreg) were identified by selecting the cluster with CD68^{+}/ITGAM^{+}/CD163^{hi}/TREM2^{hi} TAM. M1 were identified by CD68^{+}/ITGAM^{+}/CD163^{lo}/TREM2^{lo}. (*F*) Violin plots demonstrated that GPNMB was expressed on Mreg and not on M1-like macrophages. (*G*) Mreg (mainly SPM) and M1-like macrophages (mainly LPM) pathway enrichment determined by GSEA.

demonstrated that the SPM gene signature was consistently present in all tumors. The t-distributed stochastic neighbor embedding (t-SNE) plots of macrophage cluster identified by genes *CD68*, *ITGAM*, *CD163*, and *MRC1* showed dramatic overexpression of 14 SPM genes in both pleural effusion and tumor tissue (Fig. 7 *A* and *B* and *SI Appendix*, Fig. S15). Gene expression violin plots of SPM genes were consistently higher in macrophages than in other clusters (Fig. 7 *C* and *D* and *SI Appendix*, Fig. S15). We identified five genes, *GPNMB, STAB1, TREM2, LAIR1*, and *MARCO* that were upregulated transmembrane proteins expressed by SPM phenotypic TAM and could be potential therapeutic targets for immunotherapy. Mouse SPM genes *Clen4n*, *Cbr2*, and *Tns1* were excluded due to the absence of these genes in human. In contrast to SPM, the expression of LPM gene profiles was less specific, supporting the potential plasticity of macrophages originating from local tissues (*SI Appendix*, Figs. S16 and S17).

TREM2 defines a group of macrophages with regulatory function (Mreg), which could be an important therapeutic target in mesothelioma as well as other solid tumors (32, 33). We therefore characterized this population more specifically. We observed that the 94% of TAM in tumor biopsy from untreated mesothelioma are Mreg (Fig. 7*E*). GPNMB was also overexpressed in Mreg and absent in M1-like TAM (Fig. 7*F*). Enrichment pathways determined by GSEA in Mreg (mainly SPM) and M1-like TAM (mainly LPM) largely overlapped with those observed in mouse data (Fig. 7*G*).

Trem2 Knockout (KO) Results in M2-Like SPM Depletion and Unfavorable Tumorigenesis. Considering that TREM2 was one of the most specific markers for SPM and that it is highly expressed in human untreated mesothelioma, we tested its impact on tumorigenesis using Trem2 KO mice. In vivo data demonstrated a dramatic reduction of M2-like SPM and mesospheres in Trem2KO mice compared with WT mice (Fig. 8). At 4 wk after *ip* challenge of RN5 cells, tumor nodules could be observed on the diaphragm in both groups, but less invasion and smaller tumors were found in the Trem2KO mice (Fig. 8 *A* and *B*). The number of mesospheres was significantly lower (Fig. 8*C*). F4/80^{lo}CD206^{+} M2-like SPM nearly disappeared, while F4/80^{hi}CD206^{-} LPM were more readily visible in the Trem2KO mice compared with WT mice (Fig. 8*D*). Flow cytometric data showed that CD11b^{lo}F4/80^{lo} SPM significantly decreased, while CD11b^{hi}F4/80^{hi} LPM significantly increased in the Trem2KO mice compared with WT mice (Fig. 8 *E* and *F*). The proportion of CD206^{+} TAM was significantly lower for both SPM and LPM in the Trem2KO mice compared to WT mice (Fig. 8*G*).

Taken together, these results demonstrate that Trem2 depletion leads to reduction in CD206^{+} M2like TAM and is associated with an unfavorable tumorigenesis. Trem2 depletion is also associated with a drop in SPM and a compensatory increase in LPM.

Discussion

Most TAM originate either from monocytes or from tissue-resident macrophages (7, 8). Their distinction is often difficult due to a lack of specific surface markers (34, 35). The peritoneal and pleural cavities have the unique ability to separate macrophages into SPM and LPM (11, 12). In this series of experiments, we observed that monocyte-derived SPM played a predominant role in the development of mesothelioma. The time course demonstrated that SPM were the first population to infiltrate the tumor and generated the vast majority of CD206^{+} M2-like TAM. We also observed that the upregulation of SPM preceded the upregulation of MDSC and was followed by a drop in T and B cells. Systemic macrophage depletion with CL decreased tumor progression and reduced cytokines, chemokines, and growth factors in the peritoneal cavity. CCL2 expression remained high supporting the possibility that this chemokine is a key mediator in recruiting monocytes to the tumor microenvironment (12, 36). More specific deletion of M2-like TAM by the conditional deletion of Dicer1 in myeloid cells led to rejection of the tumor in the *sc* and *ip* model. This was associated with the downregulation of PD-L1 on SPM and LPM. Further experiments demonstrated that CD206^{+} SPM isolated from the peritoneal cavity of tumor-bearing mice facilitated tumor development in vivo and in vitro, while LPM did not.

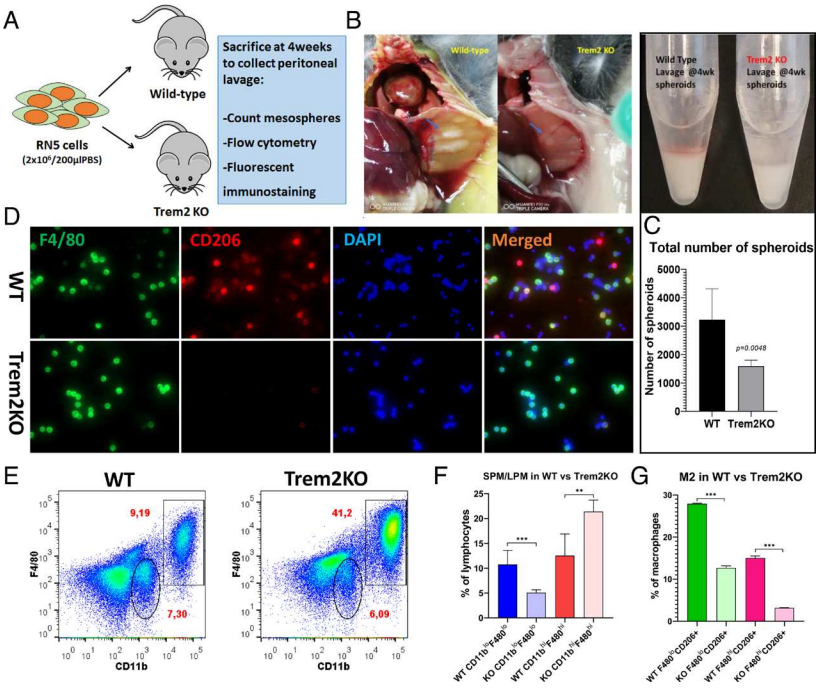

Fig. 8. Trem2 KO results in M2 SPM depletion and unfavorable tumorigenesis (*A*) Experimental schema: RN5 cells (2 × 10^6/200 µL PBS) were injected ip into WT and Trem2KO C57BL/6 mice. (*B*) Tumor modules invasion was detected when mice were killed at 4 wk after tumor challenge. Invasive tumor nodules were observed on the diaphragm in both groups, but smaller tumors were found in the Trem2KO mice. (*C*) The number of mesospheres was significantly lower in Trem2KO mice compared with WT mice, and (*D*) F4/80^{lo}CD206^{+} M2 SPM almost disappeared, whereas the F4/80^{hi}CD206^{-} LPM were more easily visible in the Trem2KO mice compared with WT mice. (*E*) Representative dot plots of flow cytometry data, showing that CD11b^{lo}F4/80^{lo} SPM decreased while CD11b^{hi}F4/80^{hi} LPM increased. (*F*) Quantification of total SPM and LPM in Trem2KO vs. WT mice. (*G*) The CD206 expression decreased in both SPM and LPM subpopulations of the Trem2KO vs. WT mice. *P < 0.05, **P < 0.01, ***P < 0.001, ****P < 0.0001.

These observations therefore suggest that monocyte-derived M2-like SPM are critical in the development of mesothelioma.

Microarray and scRNA-seq data demonstrated that SPM and LPM shared some common mechanisms in the tumor microenvironment with the activation of the IL-2-STAT5 signaling pathway, promotion of an inflammatory response and EMT. However, LPM were involved in the IFN-γ response, while SPM activated the KRAS and TNF-α/NFkB signaling pathways. This observation suggests that LPM are more efficient in activating the T cell response, which may explain why their presence in the tumor microenvironment may translate into better outcome in the peritoneal model.

The potential immune benefit generated by LPM was demonstrated by the loss of the immune protection in a memory model after the intrapleural injection of CL. In this mouse model, *sc* mesothelioma tumor treated with a short course of oligofractionated nonablative radiation 7 d before surgery developed a systemic antitumoral immune response mediated by memory CD4 and CD8 T cells (22). These mice were therefore resistant to tumor development in the pleural cavity. After intrapleural injection of CL, however, LPM were profoundly depleted, while SPM rapidly recovered, and mice lost their immune protection. The tumor grew relatively slowly compared to naïve mice suggesting that the memory response was still effective, but not as efficient. Increasing evidence demonstrate that tissue-resident macrophages play a key role in promoting organ surveillance by supporting both the CD4 and CD8 memory T cell response locally (24, 37). This observation is important considering that the antitumoral immune response is predominantly driven by memory T cells (38). Therefore, the maintenance of tissue-resident macrophage in the tumor microenvironment, while targeting monocyte-derived TAM could be the most optimal approach.

Using D$^{-/-}$ mice, we demonstrated that M2-like TAM were a critical component in the development of mesothelioma. In fact, the specific deletion of M2-like TAM was associated with tumor rejection both in the *sc* and *ip* model and the gene expression profile demonstrated that the TCR, BCR, TGF-β, Wnt, and p53 signaling pathways were restored. One of the main pathways that remained dysregulated was the PI3k-Akt-mTOR signaling pathway, suggesting that a combined therapeutic approach specifically targeting M2-like TAM and the PI3K-Akt-mTOR signaling pathway could be beneficial. Previous studies have shown that the PI3K-Akt-mTOR signaling pathway is upregulated in mesothelioma and could be a potential therapeutic target (39, 40).

Considering the importance of differentiating SPM and LPM and the importance to specifically target SPM for therapy, we then identified a specific gene signature for the SPM and the LPM subpopulations. These gene signatures were then applied to patients with mesothelioma using scRNA-seq. The analysis from human samples confirmed the potential value of the gene signature to identify monocyte-derived M2-like TAM in patients with mesothelioma. All the genes identified on SPM were highly expressed by the macrophage population isolated from the pleural effusion and the tumor, supporting the notion that TAM are predominantly originating from monocytes in pleural mesothelioma (41, 42). This analysis allowed us to identify TREM2, STAB1, LAIR1, MARCO, and GPNMB as potential targets for immunotherapy in the clinical setting. Some of these genes have also been identified in single-cell analysis from human lung adenocarcinoma (43).

Among these five potential targets, TREM2 is highly expressed in mesothelioma and was recently demonstrated to be an important target for monocyte-derived TAM in other solid tumors (32, 44). We therefore tested its impact in our preclinical model using Trem2KO mice. We observed that Trem2 deletion was associated with impaired tumorigenesis. Of particular importance is the fact that Trem2 deletion led to an overall reduction in SPM and compensatory increase in LPM. Considering that LPM are mediating the IFN-γ response, the shift from SPM to LPM may explain why Trem2 deletion is associated with enhanced CD8 T cell infiltration in the tumor and more efficient anti-programmed cell death protein 1 (PD-1) therapy (33, 45). This observation is also consistent with the concept that Trem2$^{+/+}$ TAM are immunosuppressive and Trem2$^{-/-}$ TAM are immunostimulatory (46). Our data on hallmark gene sets consistently demonstrated that the activated pathways in SPM (mainly Mreg-CD68^{+}/TREM2^{hi}) were immunosuppressive, while the activated pathways in LPM (mainly M1-CD68^{+}/TREM2^{lo}) were immunostimulatory.

Targeting specific TAM populations could potentially be more efficient and provide greater benefit than targeting colony stimulating factor 1 receptor (CSF-1R) in the clinical setting (47). A more selective approach could also provide the ability to reverse the TAM polarization from an anti-inflammatory M2-like phenotype to a proinflammatory M1-like phenotype, which can lead to better and more persistent activation of the antitumoral immune response (25). This was demonstrated in the combination of αCSF-1R with αCD40 therapy (48). The macrophage depletion with αCSF-1R took 1 wk during which αCD40 activated the tumor microenvironment. Afterward, the rapid repopulation of TAM was redirected toward an M1-like response with synergistic benefit on the tumor response.

This study presents limitations related to potential overlap between SPM and LPM. However, the two cell populations were sufficiently distinct to be able to identify a gene signature profile that was different. Further studies will also be required to characterize the interaction between the LPM and the memory T cell response in more details. Also, the LPM population behaved differently in the peritoneal cavity than the pleural cavity, and it will be of importance to determine whether this can explain the difference in survival between pleural and peritoneal mesothelioma.

In conclusion, this study demonstrates the importance of the SPM and LPM phenotypes in mesothelioma. The SPM population is a critical component in tumor progression. SPM-like TAM could thus be an important target for immunotherapy in clinical trials, particularly in combination with immune checkpoint blockade. This approach could provide major benefit in mesothelioma.

Materials and Methods

Murine mesothelioma cells and mouse models were employed to investigate systemic depletion of macrophages with CL and determine cytokines and chemokines in peritoneal lavage by enzyme-linked immunosorbent assay (ELISA). The selective depletion of M2-like macrophages was performed in conditional depletion of Dicer 1 mice. Cell populations and characteristics were analyzed by flow cytometry, cell sorting, and fluorescent immunostaining. Samples from mouse and patients with mesothelioma were used to do microarray assay, or scRNA-Seq analysis. GSEA and Molecular Signature Database were performed using online platforms. Statistical analysis was conducted in each experiment. This study was approved by the University Health Network Research Ethics Board (REB#19-5858) and all patients signed the consent forms. All detailed methods were included as *SI Appendix*.

Data, Materials, and Software Availability. All study data are included in the article and/or *SI Appendix*. The GSEA files have been uploaded to a public repository and are available at https://figshare.com/articles/dataset/A_microarray_F480lo_F480hi_RN5vsN_all_genes_xlsx/21304617 (49).

ACKNOWLEDGMENTS. This work was supported by the Mesothelioma Applied Research Foundation, the Princess Margaret Cancer Foundation, and the University Health Network (UHN) Foundation. M.de Perrot is the recipient from the Canadian Mesothelioma Foundation Professorship in Mesothelioma Research.

Author affiliations: [a]Latner Thoracic Surgery Research Laboratories, Division of Thoracic Surgery, Toronto General Hospital, Toronto General Hospital Research Institute, University Health Network, University of Toronto, Toronto, ON M5G 1L7, Canada; [b]Princess Margaret Cancer Centre, University Health Network, Toronto, ON M5G 1L7, Canada; [c]dYcode Inc., Toronto, ON L6C 2R9, Canada; [d]Department of Thoracic Surgery, University Hospitals of Geneva, Geneva 1205, Switzerland; [e]Swiss Federal Institute of Technology in Lausanne (Ecole Polytechnique Fédérale de Lausanne), Lausanne 1015, Switzerland; [f]Agora Research Cancer Centre, Lausanne 1005, Switzerland; [g]Laboratory of Molecular Oncology, University Hospital Zurich, University of Zurich, Zürich 8044, Switzerland; and [h]Department of Immunology, University of Toronto, Toronto, ON M5S 1A8, Canada

1. M. Carbone *et al.*, Mesothelioma: Scientific clues for prevention, diagnosis, and therapy. *CA Cancer J. Clin.* **69**, 402–429 (2019).
2. M. Carbone *et al.*, Medical and surgical care of patients with mesothelioma and their relatives carrying germline BAP1 mutations. *J. Thorac. Oncol.* **17**, 873–889 (2022).
3. Y. Blum *et al.*, Dissecting heterogeneity in malignant pleural mesothelioma through histo-molecular gradients for clinical applications. *Nat. Commun.* **10**, 1333 (2019).
4. B. Z. Qian, J. W. Pollard, Macrophage diversity enhances tumor progression and metastasis. *Cell* **141**, 39–51 (2010).
5. P. Courtiol *et al.*, Deep learning-based classification of mesothelioma improves prediction of patient outcome. *Nat. Med.* **25**, 1519–1525 (2019).
6. T. Blondy *et al.*, Involvement of the M-CSF/IL-34/CSF-1R pathway in malignant pleural mesothelioma. *J. Immunother. Cancer.* **8**, e000182 (2020).
7. F. R. Greten, S. I. Grivennikov, Inflammation and cancer: Triggers, mechanisms, and consequences. *Immunity* **51**, 27–41 (2019).
8. L. Cassetta *et al.*, Human tumor-associated macrophage and monocyte transcriptional landscapes reveal cancer-specific reprogramming, biomarkers, and therapeutic targets. *Cancer Cell* **35**, 588–602.e10 (2019).
9. D. W. Cain *et al.*, Identification of a tissue-specific, C/EBPbeta-dependent pathway of differentiation for murine peritoneal macrophages. *J. Immunol.* **191**, 4665–4675 (2013).
10. E. E. Ghosn *et al.*, Two physically, functionally, and developmentally distinct peritoneal macrophage subsets. *Proc. Natl. Acad. Sci. U.S.A.* **107**, 2568–2573 (2010).
11. A. Cassado Ados, M. R. D'Império Lima, K. R. Bortoluci, Revisiting mouse peritoneal macrophages: Heterogeneity, development, and function. *Front. Immunol.* **6**, 225 (2015).
12. C. C. Bain *et al.*, Rate of replenishment and microenvironment contribute to the sexually dimorphic phenotype and function of peritoneal macrophages. *Sci. Immunol.* **5**, eabc4466 (2020).
13. A. Dos Anjos Cassado, F4/80 as a major macrophage marker: The case of the peritoneum and spleen. *Results Probl. Cell Differ.* **62**, 161–179 (2017).
14. E. E. Ghosn *et al.*, Two physically, functionally, and developmentally distinct peritoneal macrophage subsets. *Proc. Natl. Acad. Sci. U.S.A.* **107**, 2568–2573 (2010).
15. T. Heidt *et al.*, Differential contribution of monocytes to heart macrophages in steady-state and after myocardial infarction. *Circ. Res.* **115**, 284–295 (2014).
16. A. S. Puranik *et al.*, Kidney-resident macrophages promote a proangiogenic environment in the normal and chronically ischemic mouse kidney. *Sci. Rep.* **8**, 13948 (2018).
17. H. H. Eum *et al.*, Tumor-promoting macrophages prevail in malignant ascites of advanced gastric cancer. *Exp. Mol. Med.* **52**, 1976–1988 (2020).
18. F. Peyraud, S. Cousin, A. Italiano, CSF-1R inhibitor development: Current clinical status. *Curr. Oncol. Rep.* **19**, 70 (2017).
19. M. Laviron, A. Boissonnas, Ontogeny of tumor-associated macrophages. *Front. Immunol.* **10**, 1799 (2019).
20. H. Rehrauer *et al.*, How asbestos drives the tissue towards tumors: YAP activation, macrophage and mesothelial precursor recruitment, RNA editing, and somatic mutations. *Oncogene* **37**, 2645–2659 (2018).
21. M. Anraku *et al.*, Synergistic antitumor effects of regulatory T cell blockade combined with pemetrexed in murine malignant mesothelioma. *J. Immunol.* **185**, 956–966 (2010).
22. T. A. Wynn, Myeloid-cell differentiation redefined in cancer. *Nat. Immunol.* **14**, 197–199 (2013).
23. J. I. Youn *et al.*, Epigenetic silencing of retinoblastoma gene regulates pathologic differentiation of myeloid cells in cancer. *Nat. Immunol.* **14**, 211–220 (2013).
24. B. T. V. Duong *et al.*, A liquid biopsy for detecting circulating mesothelial precursor cells: A new biomarker for diagnosis and prognosis in mesothelioma. *EBioMedicine* **61**, 103031 (2020).
25. K. D. Prummel *et al.*, Hand2 delineates mesothelium progenitors and is reactivated in mesothelioma. *Nat. Commun.* **13**, 1677 (2022).
26. T. Koopmans, Y. Rinkevich, Mesothelial to mesenchyme transition as a major developmental and pathological player in trunk organs and their cavities. *Commun. Biol.* **1**, 170 (2018).
27. L. De La Maza *et al.*, In situ vaccination after accelerated hypofractionated radiation and surgery in a mesothelioma mouse model. *Clin. Cancer Res.* **23**, 5502–5513 (2017).
28. J. Murakami *et al.*, Triplemodality therapy maximizes antitumor immune responses in a mouse model of mesothelioma. *Sci. Transl. Med.* **13**, eabd9882 (2021), 10.1126/scitranslmed.abd9882.
29. N. Lijima, A. Iwasaki, T cell memory. A local macrophage chemokine network sustains protective tissue-resident memory CD4 T cells. *Science* **346**, 93–98 (2014).
30. C. Baer *et al.*, Suppression of microRNA activity amplifies IFN-gamma-induced macrophage activation and promotes anti-tumour immunity. *Nat. Cell Biol.* **18**, 90–802 (2016).
31. M. Liguori *et al.*, The soluble glycoprotein NMB (GPNMB) produced by macrophages induces cancer stemness and metastasis via CD44 and IL-33. *Cell Mol. Immunol.* **18**, 711–722 (2020), 10.1038/s41423-020-0501-0.
32. Y. Katzenelenbogen *et al.*, Coupled scRNA-Seq and intracellular protein activity reveal an immunosuppressive role of TREM2 in cancer. *Cell* **182**, 872–885.e19 (2020).
33. M. Molgora *et al.*, TREM2 modulation remodels the tumor myeloid landscape enhancing anti-PD-1 immunotherapy. *Cell* **182**, 886–900.e17 (2020).
34. M. Rosas *et al.*, The transcription factor Gata6 links tissue macrophage phenotype and proliferative renewal. *Science* **344**, 645–648 (2014).
35. F. Ginhoux, M. Guilliams, Tissue-resident macrophage ontogeny and homeostasis. *Immunity* **44**, 439–449 (2016).
36. R. Y. Ma *et al.*, Monocyte-derived macrophages promote breast cancer bone metastasis outgrowth. *J. Exp. Med.* **217**, e20191820 (2020).
37. B. Stolp *et al.*, Salivary gland macrophages and tissue-resident CD8 + T cells cooperate for homeostatic organ surveillance. *Sci. Immunol.* **5**, eaaz4371 (2020).
38. J. M. Mankor *et al.*, Efficacy of nivolumab and ipilimumab in patients with malignant pleural mesothelioma is related to a subtype of effector memory cytotoxic T cells: Translational evidence from two clinical trials. *EBioMedicine* **62**, 103040 (2020).
39. R. Kanteti *et al.*, PI3 kinase pathway and MET inhibition is efficacious in malignant pleural mesothelioma. *Sci. Rep.* **6**, 32992 (2016).
40. B. K. Bitanihirwe *et al.*, PI3K/mTOR signaling in mesothelioma patients treated with induction chemotherapy followed by extrapleural pneumonectomy. *J. Thorac. Oncol.* **9**, 239–247 (2014).
41. L. A. Lievense *et al.*, Pleural effusion of patients with malignant mesothelioma induces macrophage-mediated T cell suppression. *J. Thorac. Oncol.* **11**, 1755–1764 (2016).
42. A. L. Chéné *et al.*, Pleural effusions from patients with mesothelioma induce recruitment of monocytes and their differentiation into M2 macrophages. *J. Thorac. Oncol.* **11**, 1765–1773 (2016).
43. Y. Lavin *et al.*, Innate immune landscape in early lung adenocarcinoma by paired single-cell analyses. *Cell* **169**, 750–765.e17 (2017).
44. X. Cheng *et al.*, Systematic pan-cancer analysis identifies TREM2 as an immunological and prognostic biomarker. *Front. Immunol.* **12**, 646523 (2021).
45. D. Xiong, Y. Wang, M. You, A gene expression signature of TREM2 hi macrophages and γδ T cells predicts immunotherapy response. *Nat. Commun.* **11**, 5084 (2020).
46. A. Bugler-Lamb, M. Guilliams, Myeloid cells TREM down anti-tumor response. *Cell* **182**, 796–798 (2020).
47. L. Zhang *et al.*, Single-cell analyses inform mechanisms of myeloid-targeted therapies in colon cancer. *Cell* **181**, 442–459.e29 (2020).
48. S. Hoves *et al.*, Rapid activation of tumor-associated macrophages boosts preexisting tumor immunity. *J. Exp. Med.* **215**, 859–876 (2018).
49. L. Wu, Microarray and scRNA-Seq datasets F480lo F480hi RN5vsN all genes.xlsx dataset. Figshare. https://figshare.com/articles/dataset/A_microarray_F480lo_F480hi_RN5vsN_all_genes_xlsx/21304617. Deposited 10 October 2022.